Improvement of Power Efficiency in Flapping-Wing MAVs through a Semi-Passive Motion Control Approach

Hosein Mahjoubi, and Katie Byl

***Abstract*—Among unmanned aerial systems (UASs), flapping-wing micro aerial vehicles (MAVs) are perhaps the newest field of research. Inspired by small size and agile flight of insects and birds, these vehicles offer a great potential for applications such as reconnaissance, surveillance, search and rescue, mapping, etc. Practicality of these systems however still depends on how we overcome various challenges ranging from control methodology to morphological construction and power supply. Further inspiration from solutions in nature is one way of approaching such problems. Through modeling synchronous muscles in insects [1], we have previously shown that manipulation of mechanical impedance properties at wing joints can be a very efficient method for controlling lift and thrust production in flapping-wing MAVs. In our current work, we will investigate the power requirements of this control approach through simulated flight experiments. The results indicate that these requirements are considerably lower compared to when conventional control strategies – methods that often rely on changing stroke properties such as frequency or magnitude of the flapping motion – are employed. With less power demands, we believe our proposed control strategy is able to significantly improve flight time in future flapping-wing MAVs.**

Keywords*—*Flapping-Wing MAVs; Power Efficiency; Aerial Robotics; Hummingbird Flight; Tunable Impedance; Variable Stiffness Actuator; Bio-inspired MAVs; Maneuverability.

I. Introduction

Initially introduced during World War I [2], Unmanned Aerial Vehicles (UAVs) have experienced a considerable level of growth both in military and civilian application domains. Surveillance, reconnaissance, search and rescue, traffic monitoring, fire detection and mapping are just a few examples of these applications.

UAVs can be categorized into three basic groups: fixed-wing airplanes, rotary-wing models and flapping wing systems. Each type has different advantages and disadvantages. However, as we go smaller in size to design Micro Aerial Vehicles (MAVs), the limitations of fixed and rotary-wing technologies become more apparent; the Reynolds number decreases as the wing surfaces become smaller, resulting in unsteady aerodynamic effects that are still a subject of research. On the other hand, flapping wing designs inspired by birds and insects offer the most potential for miniaturization and maneuverability.

Unparalleled dynamics, speed and agility are known traits of insects and birds that turn them into the most efficient flyers in nature. Furthermore, their ability to adapt with varying weather and environmental conditions is phenomenal; hence mimicking their flight dynamics and actuation mechanisms would be a reasonable approach to design of practical MAVs. Some of the available designs include *Harvard's Robotic Fly* [3], *Delfly* [4] and the *Entomopter* [5].

The small size of these systems poses considerable limits on available space for actuators, power supply and any sensory or control modules. Although a major portion of the overall mass is often allocated to batteries [3]-[4], the flight time of these vehicles rarely exceeds a few minutes. Thus in terms of efficiency and flight duration, current flapping-wing MAVs are still far inferior to their fixed and rotary-wing counterparts. To realize a bio-inspired flapping-wing MAV with more efficient flight time, a more in-depth study and mimicking of insect flight may be required.

Developed in Georgia Tech Research Institute, the *Entomopter* [5]-[6] is one of the few examples that steps into this next stage of bio-inspired MAV design. Instead of conventional electric motors, this system employs a novel reciprocating chemical muscle (RCM) to power the oscillatory stroke motion of each wing. This actuator uses a chemical composition as fuel. Chemical reactions can provide a much greater energy output per unit mass than current electric storage cell technology. Therefore, replacing the batteries and electric motors with RCM technology not only reduces the bulk of the system, but also may significantly improve flight time in flapping-wing MAVs.

In addition to bio-inspired stroke actuation methods such as RCM, one could also investigate possible mechanisms that insects and small birds employ to regulate aerodynamic force during various aerial maneuvers. Control strategies developed based on such mechanisms may further improve energy efficiency and flight time of future MAV prototypes. The *Tunable Impedance* (TI) method [7] is one such strategy. Inspired by the structure of antagonistic muscle pairs attached to wing joints – also known as synchronous muscles [8] – in insects and hummingbirds, we have previously shown that mechanical impedance properties of each wing joint can be modeled as a linear torsional spring [1], [9]. Tunable Impedance approach states that by manipulating the properties of these springs, it is possible to shape pitch rotation profile of each wing and indirectly adjust its mean production of lift and thrust forces [7], [10].

Unlike conventional approaches to flapping-wing MAV

H. Mahjoubi and K. Byl are with the Robotics Laboratory, Department of Electrical and Computer Engineering, University of California at Santa Barbara, Santa Barbara, CA 93106 USA (e-mail: h.mahjoubi@ece.ucsb.edu, katiebyl@ece.ucsb.edu).

control, TI does not require any modifications in flapping properties such as frequency or magnitude of stroke. This suggests that a single stroke profile can be used during all operational modes including takeoff, forward acceleration and hovering. Hence regardless of the maneuver, the MAV will need a relatively constant amount of power to maintain flapping its wings. Naturally, this amount should be large enough to provide sufficient lift for levitation.

Depending on the desired maneuver, extra power may be required to change mechanical impedance properties of each wing joint via suitable actuators [11]-[14]. Through simulated flight experiments, this work shows that such changes are often very small and do not demand considerable amounts of power. Thus with a motion controller based on Tunable Impedance approach, we expect that an actual MAV's power requirement during any maneuver remains almost constant, i.e. close to the amount necessary for hovering.

To appreciate the significance of this feature, a new set of flight experiments were simulated. In this group of experiments, wings' mechanical impedance properties were fixed and aerodynamic forces were controlled through changes in shape and frequency of flapping profile. Comparing both cases, it is observed that power requirements in the Tunable Impedance method are considerably lower. Therefore, implementation of a similar control approach on an actual MAV may significantly improve efficiency and result in longer flight times.

The remainder of this paper is organized as follows. Section II briefly explains our model of mechanical impedance in the wing joints. Power requirements for value modifications in the parameters of this model can be calculated through expressions that will be derived there. Section III reviews the employed aerodynamic model for flight simulations and demonstrates how these forces can be controlled through adjusting mechanical impedance properties of the wing joints. The MAV model and the two designed controllers are discussed in Sections IV. The results of simulated flight experiments are presented in section V. Section VI concludes this work.

II. Mechanical Impedance of the Wing Joint

In [1], we reviewed different types of muscle that various insects employ during flight. Among them, synchronous muscles [8] are the only kind that is directly attached to the wing joint (Fig. 1). Thus, they should have a key role in determining mechanical impedance of the wing joint. This mechanical impedance is responsible for regulation of changes in wing's angle of attack (AoA) in response to aerodynamic torques [1], [7]. Thus, modeling these muscles could further improve our understanding of insect flight.

A. Modeling of Muscle-Joint Connection

The antagonistic muscle pairs in Fig. 1 [15] and their

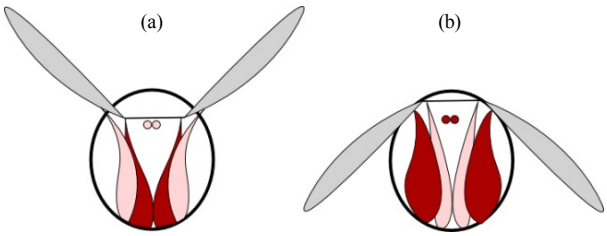

Fig. 1. An illustration of insect's wing stroke using synchronous muscles: (a) upstroke and (b) downstroke. Muscles in the process of contraction are shown in a darker color (adapted from [15]).

connection to the wing joint can be modeled by the mechanical structure illustrated in Fig. 2. The behavior of each muscle can be approximately modeled by a quadratic spring [16], i.e. its output force F is equal to:

$$F(\delta_i) = \tfrac{1}{2} A\delta_i^2 + B\delta_i + C, \qquad i = 1,2 \tag{1}$$

where A, B and C are constant coefficients and δ_i represent the corresponding change in length of each spring.

In [1], using (1) we have shown that rotational stiffness of the joint in Fig. 2 is derived as:

$$k_{rot} = 2R^2\ (Ax_c + B) \tag{2}$$

Here, R is the radius of the joint and x_c represents the displacement due to co-activation of antagonistic muscle pair, i.e.:

$$x_c = \tfrac{1}{2}(x_1 + x_2) \tag{3}$$

The displacement induced by actuator force F_{Mi} on the input end of each spring is shown by x_i. The differential displacement of these springs, i.e. x_d, is responsible for adjustment of wing's equilibrium pitch angle ψ_0:

$$x_d = \tfrac{1}{2}(x_1 - x_2) = R\psi_0 \tag{4}$$

It was also shown [1] how an external torque τ_{ext} influences the pitch angle ψ of the wing joint:

$$\tau_{ext} = k_{rot}\ (\psi - \psi_0) \tag{5}$$

Hence, the wing joint can be considered as a torsional spring whose stiffness and set point are respectively controlled through co-activation and differential activation of an antagonistic synchronous muscle pair. In Section III.B

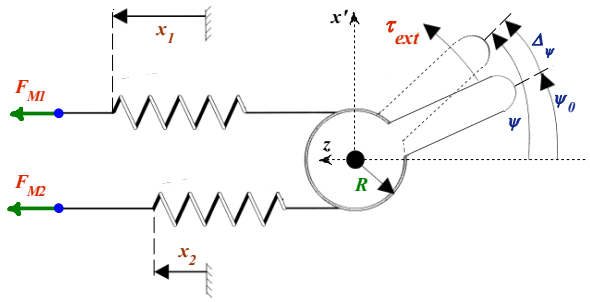

Fig. 2. A simplified mechanical model of synchronous muscle-joint structure. Each muscle is modeled by a quadratic spring. A force of F_{Mi} pulls the input end of each spring, resulting in the displacement x_i. The other sides of both springs are attached to a pulley of radius R which models the joint.

we show how these parameters influence lift and thrust.

B. Active Impedance Regulation: Power Requirements

Contraction of synchronous muscle pairs may change both stiffness and equilibrium position of the wing joint. Like all other muscles, these contractions consume energy. In Fig. 2, integration of (1) with respect to δ_i shows how much work W is required to change the length of each spring:

$$W(\delta_i) = \tfrac{1}{6} A \delta_i^3 + \tfrac{1}{2} B \delta_i^2 + C \delta_i \quad i = 1,2 \tag{6}$$

Since:

$$\delta_1 = x_c - R\ (\psi - \psi_0) \tag{7}$$

$$\delta_2 = x_c + R\ (\psi - \psi_0) \tag{8}$$

from (2) and (4) the overall work is equal to:

$$W(\delta_1) + W(\delta_2) = 2W(x_c) + \tfrac{1}{2} k_{rot}\ (\psi - \psi_0)^2 \tag{9}$$

The required power for impedance manipulation, i.e. P_{TI} is then calculated by differentiating (9) with respect to time:

$$P_{TI} = 2F(x_c)\dot{x}_c + \tfrac{1}{2}\dot{k}_{rot}\ (\psi - \psi_0)^2 - k_{rot}\ (\psi - \psi_0)\dot{\psi}_0 \tag{10}$$

Using (1)-(2), it is easy to show that choosing $C = 0.5B^2/A$:

$$F(x_c)\dot{x}_c = \tfrac{1}{16 A^2 R^6} k_{rot}^2 \dot{k}_{rot} \tag{11}$$

which is replaced in (10) to yield:

$$P_{TI} = \tfrac{1}{8 A^2 R^6} k_{rot}^2 \dot{k}_{rotc} + \tfrac{1}{2}\dot{k}_{rot}\ (\psi - \psi_0)^2 - k_{rot}\ (\psi - \psi_0)\dot{\psi}_0 \tag{12}$$

The last expression allows us to estimate power requirements for manipulation of k_{rot} and ψ_0 based on instantaneous values of these parameters and their time derivatives. In Section V, we will use (12) for power estimation during simulated flight experiments with Tunable Impedance controller.

III. Aerodynamic Forces

With low Reynolds numbers, aerodynamics of insect flight has become an active field of research over the past several decades [17]-[21]. Various unsteady-state mechanisms have been identified that depending on the species, demonstrate different amounts of contribution to production of aerodynamic force. Among these phenomena, three mechanisms are the most significant in many flying insects: *delayed stall* [18], *rotational circulation* [18]-[19], and *wake capture* [17]-[18]. Experimental data have been used to develop mathematical expressions for estimation of forces produced by these mechanisms [18], [22]-[23]. We have previously used these results to model the overall aerodynamic force in a dragonfly/hummingbird scale flapping-wing MAV [1]. Here, we will only repeat the final equations and then proceed to explain the interaction between aerodynamic force and mechanical impedance of the wing joint. For further details, reading [1] and [22] is encouraged.

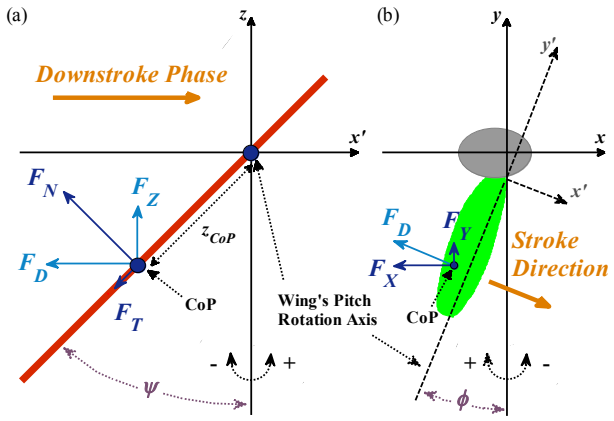

Fig. 3. (a) Wing cross-section (during downstroke) at center of pressure, illustrating the pitch angle ψ. Normal and tangential aerodynamic forces are represented by F_N and F_T. F_Z and F_D represent the lift and drag components of the overall force. (b) Overhead view of the wing/body setup which demonstrates the stroke angle ϕ. F_X and F_Y are components of F_D which represent forward and lateral thrust, respectively.

A. Wing Shape and Aerodynamic Forces

The components of aerodynamic force at center of pressure (CoP) of the wing are illustrated in Fig. 3.a. In this diagram, pitch angle of the wing is represented by ψ. The stroke profile of the wing – i.e. the angle ϕ in Fig. 3.b – is assumed to be sinusoidal:

$$\phi = \phi_0 \cos(2\pi\ f_s t) \tag{13}$$

where ϕ_0 is the magnitude of stroke and f_s represents flapping frequency.

Using the quasi-steady-state aerodynamic model of [1] along with Blade Element Method (BEM) [19], [24]-[25], the aerodynamic force for the wing shape of Fig. 4 can be estimated by:

$$F_N = 0.0442\rho\ (C_N(\psi)\ \dot{\phi} + 1.3462\dot{\psi})\ \dot{\phi}\ R_W^4 \tag{14}$$

$$F_T = 0.0442\rho\ C_T(\psi)\ \dot{\phi}^2 R_W^4 \tag{15}$$

where ρ is the density of air and R_W represents the span of the wing (Fig. 4). As illustrated in Fig. 3.a, F_N and F_T are the normal and tangential components of the aerodynamic force with respect to the surface of the wing. C_N and C_T are

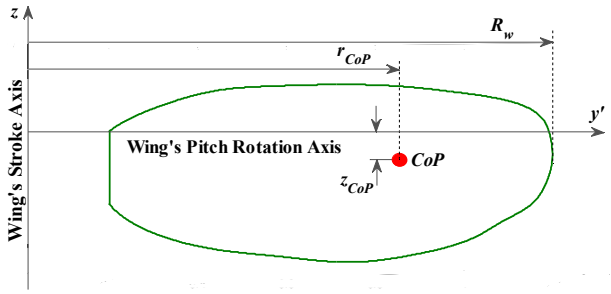

Fig. 4. The wing shape used in aerodynamic model and flight simulations. The span of the wing is represented by R_w.

angle dependent aerodynamic coefficients [1], [18]:

$$C_N(\psi) = 3.4\cos\psi \tag{16}$$

$$C_T(\psi) = \begin{cases} 0.4\cos^2(2\psi), & |\psi| \geq \frac{\pi}{4}\ rad \\ 0, & otherwise \end{cases} \tag{17}$$

Lift (F_Z) and drag (F_D) components of the aerodynamic force are calculated as follows:

$$F_Z = -F_N \sin\psi - F_T \cos\psi \tag{18}$$

$$F_D = -F_N \cos\psi + F_T \sin\psi \tag{19}$$

Forward (F_X) and lateral (F_Y) thrust are also defined as illustrated in Fig. 3.b:

$$F_X = F_D \cos\phi \tag{20}$$

$$F_Y = -F_D \sin\phi \tag{21}$$

Finally, it is important to note that center of pressure in Fig. 4 is located [1] at:

$$z_{CoP} = 0.0673\ R_W \tag{22}$$

$$r_{CoP} = 0.7221\ R_W \tag{23}$$

B. *Pitch Rotation of the Wing: A Force Control Strategy?*

In Fig. 3.a, the overall external torque that tends to change the pitch angle ψ of the wing is given by:

$$\tau_{ext} = z_{CoP} F_N - b_\psi \dot{\psi} - J_\psi \ddot{\psi} \tag{24}$$

J_ψ and b_ψ are the moment of inertia and passive damping coefficient of the wing around its pitch rotation axis, respectively. Resistance of the joint against this rotation defines mechanical impedance according to (5). Therefore, passive evolution of ψ must maintain balance between (5) and (24), i.e. ψ must satisfy:

$$J_\psi \ddot{\psi} + b_\psi \dot{\psi} + k_{rot}\ (\psi - \psi_0) - z_{CoP} F_N = 0 \tag{25}$$

Equation (25) can be numerically solved along with (14) to calculate changes in ψ and F_N for any stroke profile and mechanical impedance parameters. Other aerodynamic profiles will then be available via (15) and (18)-(21).

The values of constant physical parameters are listed in Table I. Since our MAV model is roughly the same size as an average hummingbird, stroke parameters during hovering flight are set to $\phi_0 = 60^\circ$ and $f_s = 25$ Hz [8]. Also like a hummingbird, our MAV model has two wings and in this work it is assumed that they have always the same stroke profiles and mechanical impedance properties. Under these assumptions, symmetry dictates that overall lateral thrust and roll/yaw torques are zero; hence motion is effectively limited within sagittal plane. This allows us to concentrate only on lift F_Z and forward thrust F_X of a single wing. Roll and yaw responses of the model are previously investigated in [1], [26].

Although these forces are time-dependent, their average values remain constant as long as mechanical impedance properties and stroke parameters are unperturbed [1]. We can use these mean values to investigate the influence of impedance/stroke parameters in lift/thrust production.

TABLE I
PHYSICAL PARAMETERS USED IN SIMULATIONS OF SECTION III

Symbol	Description	Value
ρ	air density at sea level	1.28 kg/m^3
R_W	span of each wing in an average hummingbird	8×10^{-2} m
J_ψ	calculated moment of inertia (pitch rotation) for the wing in Fig. 4 (wing mass = 2×10^{-4} kg)	1.564×10^{-8} N.m.s^2
b_ψ	passive damping coefficient of each wing (pitch rotation)	5×10^{-6} N.m.s
m_{body}	estimated mass of a two-winged MAV with hummingbird dimensions	4×10^{-3} kg
g	standard gravity at sea level	9.81 m/s^2

Fig. 5.a and b illustrate the changes in mean F_Z and F_X of a single wing as various k_{rot} and ψ_0 pairs are examined. All force values are normalized by the weight of the model. When $\psi_0 = 0^\circ$, instantaneous forward thrust has an almost odd-symmetric profile in every stroke cycle [1] which results in an approximately zero mean value regardless of the selected k_{rot} (Fig. 5.c). On the other hand, mean value of lift significantly varies as k_{rot} is changed. Particularly, when $k_{rot} = k_{op} = 3.92\times10^{-3}$ N.m/rad, two wings will be able to produce just enough lift – i.e. 0.5 g-Force per wing – to levitate the model. Therefore, we choose this point as the nominal mechanical impedance values for hovering. Note that when $k_{rot} = k_{op}$, small changes in ψ_0 slightly influence mean lift but also result in significant nonzero values of mean thrust (Fig. 5.d).

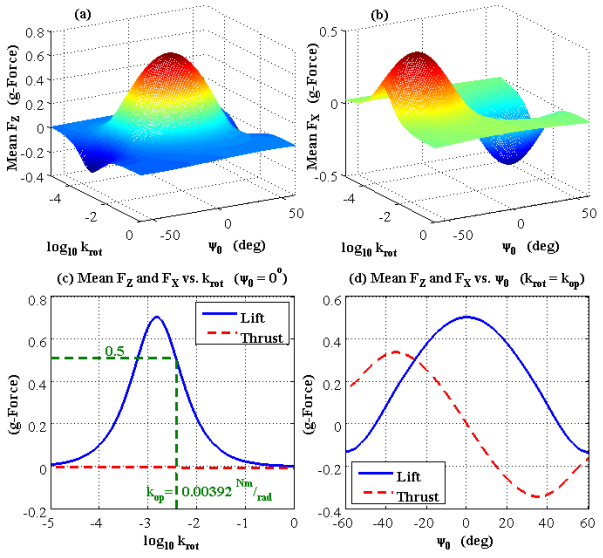

Fig. 5. (a) Mean F_Z vs. k_{rot} and ψ_0. (b) Mean F_X vs. k_{rot} and ψ_0. (c) Mean values of F_Z and F_X vs. k_{rot} when $\psi_0 = 0^\circ$. At $k_{rot} = k_{op} = 3.92\times10^{-3}$ N.m/rad, two wings are able to produce just enough lift to levitate the model. (d) Mean values of F_Z and F_X vs. ψ_0 when $k_{rot} = k_{op}$. All force values are normalized by the weight of the model. Stroke profile is always sinusoidal with constant parameters: $\phi_0 = 60^\circ$ and $f_s = 25$ Hz.

Fig. 5.c-d motivate a force/motion control strategy based on manipulation of mechanical impedance parameters around $k_{rot} = k_{op}$ and $\psi_0 = 0^\circ$. We have previously explored the high potential of this approach – also known as Tunable Impedance method – in handling agile flight maneuvers [1] through decoupled control of vertical and horizontal motions [27]. The present work will concentrate on flight efficiency and power requirements of this approach.

Power requirements in Tunable Impedance method will be compared to a conventional ad hoc control approach that manipulates frequency and shape of the stroke profile to adjust production of aerodynamic forces. From (13)-(15), the magnitude of overall instantaneous aerodynamic force is approximately a quadratic function of f_s. This relationship can also be observed in Fig. 6.a where changes in mean lift and thrust vs. f_s are plotted for constant mechanical impedance values, i.e. $k_{rot} = k_{op}$ and $\psi_0 = 0^\circ$.

From this diagram, stroke frequency can be used to control lift. However, mean thrust is unaffected by changes in f_s. Note that as long as $\psi_0 = 0^\circ$ and ϕ has a perfect sinusoidal waveform, thrust profile over one stroke cycle remains odd-symmetric [1]. Therefore, mean thrust will be close to zero. One way of producing nonzero thrust values is to employ asymmetric stroke profiles. This method is also known as *Split Cycle* [28].

Normally, upstroke and downstroke in one cycle take the same amount of time and their individual thrusts are equal and in opposite directions. By increasing the flapping speed in one part and reducing it in the other, it is possible to disturb this balance and create forward or backward thrust. To this end, we define T_{ds} as the ratio of time spent for downstroke to duration of the full stroke cycle. By definition, $T_{ds} = 0.5$ is equivalent to a symmetric stroke profile and zero mean thrust. Fig. 6.b shows that a 20% change in this value slightly increases mean lift, but at the same time, a mean thrust of approximately 0.25 g-Force per wing will be achievable. Hence simultaneous manipulation of f_s and T_{ds} can be used as a direct approach to force/motion control in flapping-wing MAVs.

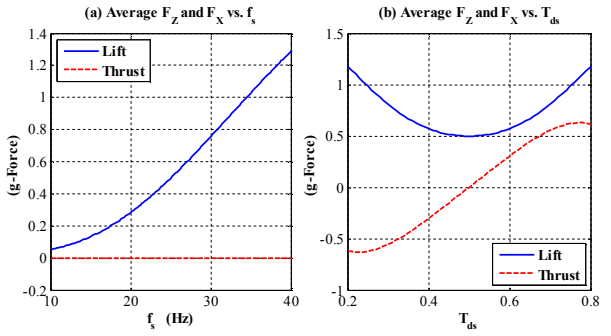

Fig. 6. (a) Mean values of F_Z and F_X vs. f_s when $T_{ds} = 0.5$. At $f_s = 25$ Hz, two wings are able to produce just enough lift to levitate the model. (b) Mean values of F_Z and F_X vs. T_{ds} when $f_s = 25$ Hz. All force values are normalized by the weight of the model. Mechanical impedance parameters are always constant: $k_{rot} = k_{op}$ and $\psi_0 = 0^\circ$.

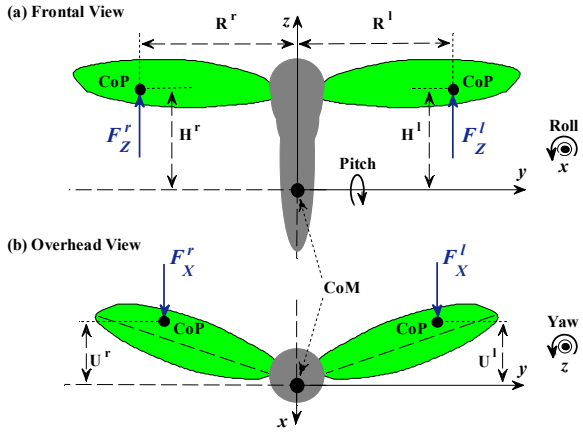

Fig. 7. Free-body diagram model of a flapping-wing MAV: (a) frontal and (b) overhead views. H, R and U are the distance components of center of pressure (CoP) of each wing from center of mass (CoM) of the model. For simulation purposes, Euler angles in Tait-Bryan ZXY convention are employed to update the orientation of the body.

IV. MAV Model and Flight Control

Fig. 7 illustrates a typical free-body diagram of a two-winged flapping-wing MAV. A 6 degree-of-freedom (6DoF) mathematical model can be derived in this body frame [1] by employing Newton's equations of motion. Physical parameters of this model are reported in Table II. In calculating the values of moment of inertia, the body was assumed to be a cylinder of radius $0.1\,R_W$ and height $1.5\,R_W$.

Based on discussions in Section III.B, two different controllers are designed for this model. In the remainder of this section, we will review the details and structure of these controllers.

A. Controller 1: Tunable Impedance

The block diagram in Fig. 8 shows how the Tunable Impedance controller is organized. To design the lift and thrust controllers, first the linear transfer function from each mechanical impedance parameter to average value of corresponding force is found through system identification experiments around $k_{rot} = k_{op}$ and $\psi_0 = 0^\circ$ [27]. LQR gains are then calculated for the approximated linear system from

TABLE II
Characteristics of the Modeled Flapping-Wing MAV

Symbol	Description	Value
b_ω	passive damping coefficient of the body (rotation)	3×10^{-3} N.m.s
b_v	viscous friction coefficient of the body when moving in the air	4×10^{-4} N.s^2/m^2
$J_{pitch}=J_{roll}$	pitch and roll moments of inertia of the body relative to CoM	4.38×10^{-6} N.m.s^2
J_{yaw}	yaw moment of inertia of the body relative to CoM	1.15×10^{-7} N.m.s^2
$H(\psi=0^\circ)$	distance of CoP from transverse plane of the body (xy in Fig. 7) when $\psi=0^\circ$	2.89×10^{-2} m
$R(\phi=0^\circ)$	distance of CoP from sagittal plane of the body (xz in Fig. 7) when $\phi=0^\circ$	5.78×10^{-2} m
$U(\phi=0^\circ)$	distance of CoP from coronal plane of the body (yz in Fig. 7) when $\phi=0^\circ$	5.8×10^{-3} m
W_{body}	body width at the base of wings	1.16×10^{-2} m

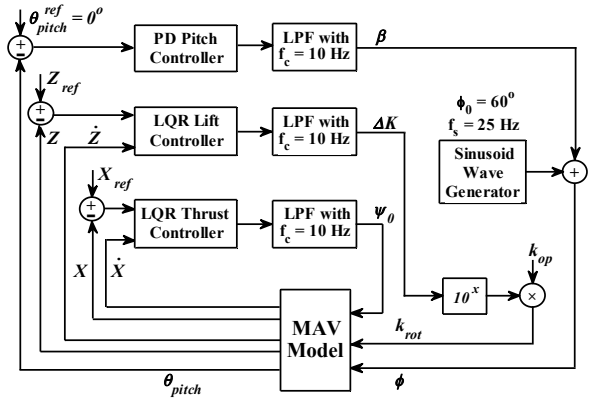

Fig. 8. Block diagram of the proposed Tunable Impedance motion controller in interaction with MAV model. Cutoff frequency f_c of each low-pass filter is set to 10 Hz. Both wings employ similar values of β, k_{rot} and ψ_0 at all times. The stroke profile properties are always constant: $\phi_0 = 60^\circ$, $f_s = 25$ Hz and $T_{ds} = 0.5$.

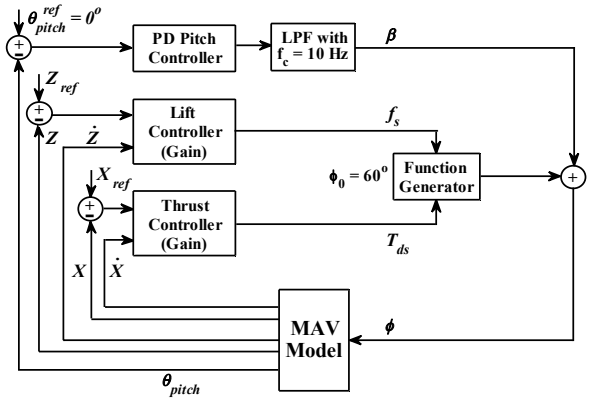

Fig. 9. Block diagram of controller 2 in interaction with MAV model. Both wings employ similar values of β, f_s and T_{ds} at all times. The magnitude of stroke and mechanical impedance parameters are always constant: $\phi_0 = 60^\circ$, $k_{rot} = k_{op}$ and $\psi_0 = 0^\circ$.

mechanical impedance parameters to vertical/horizontal position and velocity:

$$\Delta K = 25(Z - Z_{ref}) + 2\dot{Z} \tag{26}$$

$$k_{rot} = k_{op} 10^{\Delta K} \tag{27}$$

$$\psi_0 = 2000(X - X_{ref}) + 100\dot{X} \tag{28}$$

where X and Z are respectively the horizontal and vertical positions of the model in sagittal plane. X_{ref} and Z_{ref} define the reference trajectory of motion within this plane. To reduce coupling (Fig. 5.c-d), the outputs of these controllers are chosen to be limited such that $k_{rot} \in [0.2, 2] \times 10^{-2}$ N.m/rad and $|\psi_0| \leq 20^\circ$. Presence of low-pass filters on the outputs further improves decoupling [27].

Pitch angle of the body θ_{pitch} tends to be unstable. To keep this angle small, i.e. to maintain the upright orientation of the model, we chose to bias the stroke profile with a variable amount represented by β. The details of this control mechanism are discussed in [1]. The value of β is adjusted by a PD sub-controller which is tuned to 10+0.05s through trial and error. The output of this controller is limited such that $|\beta| \leq 15^\circ$.The stroke profile properties of both wings are always constant: $\phi_0 = 60^\circ$, $f_s = 25$ Hz and $T_{ds} = 0.5$.

B. Controller 2: Frequency Manipulation and Split Cycle

In the second approach, mechanical impedance parameters are always constant: $k_{rot} = k_{op}$ and $\psi_0 = 0^\circ$. Here, lift and thrust are respectively controlled through changes in f_s and T_{ds}. Fig. 9 demonstrates the block diagram of the whole controller. The pitch sub-controller in this schematic is identical to the one described earlier for controller 1. The outputs of other sub-controllers are calculated as:

$$f_s = 25 - 187.5(Z - Z_{ref}) - 12.5\dot{Z} \tag{29}$$

$$T_{ds} = 0.5 - 2.5(X - X_{ref}) - 0.2\dot{X} \tag{30}$$

and are limited to $f_s \in [14.3, 28.5]$ Hz and $T_{ds} \in [0.4, 0.6]$. The gains in (29) and (30) are tuned via trial and error such that in both control methods, simulated MAV responses to similar references remain close. The limits on f_s and T_{ds} are imposed to restrict achievable values of aerodynamic forces within the same range as controller 1 (Fig. 6.a-b).

The output of the function generator in Fig. 9 is originally a sinusoid of constant magnitude $\phi_0 = 60^\circ$ and variable frequency f_s. Depending on the value of T_{ds}, this waveform is further manipulated such that two consecutive half-cycles have unequal durations.

V. Simulated Flight Experiments

Various trajectory tracking experiments have been simulated with both controllers of Section IV. The reference trajectories were always limited to *XZ* plane, resulting in insignificant amounts of drift along the *Y*-axis. All changes in roll and yaw angles of the model were also negligible.

Some of these results are presented here to compare flight performance and power requirements. To estimate stroke power in both sets of experiments, stroke torque of each wing is calculated first:

$$\tau_{stroke} = F_D r_{CoP} + b_\phi \dot{\phi} + J_\phi \ddot{\phi} \tag{31}$$

$b_\phi = 1 \times 10^{-5}$ Nms is the passive damping coefficient of each wing when rotating around its stroke axis. J_ϕ represents the wing's moment of inertia along the stroke axis. The calculated value for this parameter is equal to 4.894×10^{-7} Nms^2 (Fig. 4 with wing mass = 2×10^{-4} kg).

The energy required for both wings to follow a specific stroke profile, i.e. E_{stroke} is then estimated by:

$$E_{stroke} = 2\int_0^t |\tau_{stroke}\, \dot{\phi}|\, dt \tag{32}$$

Since actuation in the second control approach is only limited to changes in stroke profile, (32) is in fact an estimate of this method's overall energy consumption. As for controller 1, changes in mechanical impedance properties require extra power. Using (12), total energy consumption in this approach, i.e. E_{TI} is estimated by:

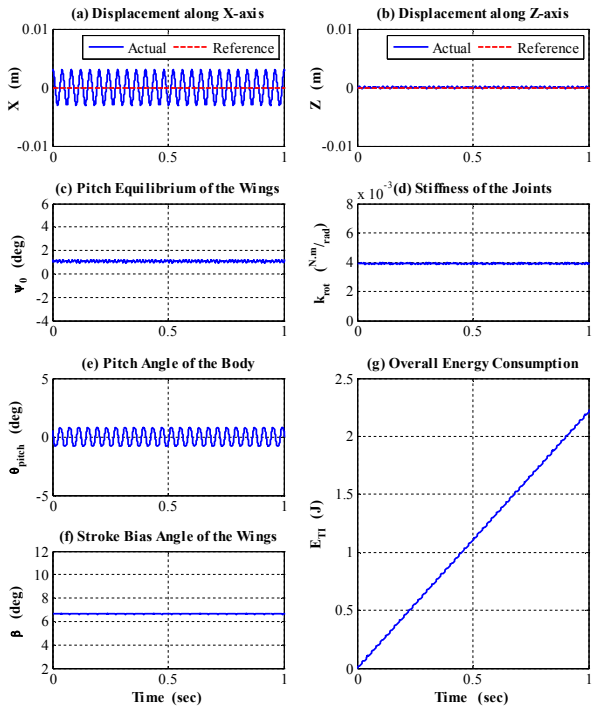

Fig. 10. Simulated results for hovering with controller 1: (a) displacement along X and (b) Z axes, (c) pitch equilibrium of the wings ψ_0, (d) stiffness of the joints k_{rot}, (e) pitch angle of the body θ_{pitch}, (f) stroke bias angle of the wings β and (g) overall energy consumption E_{TI}.

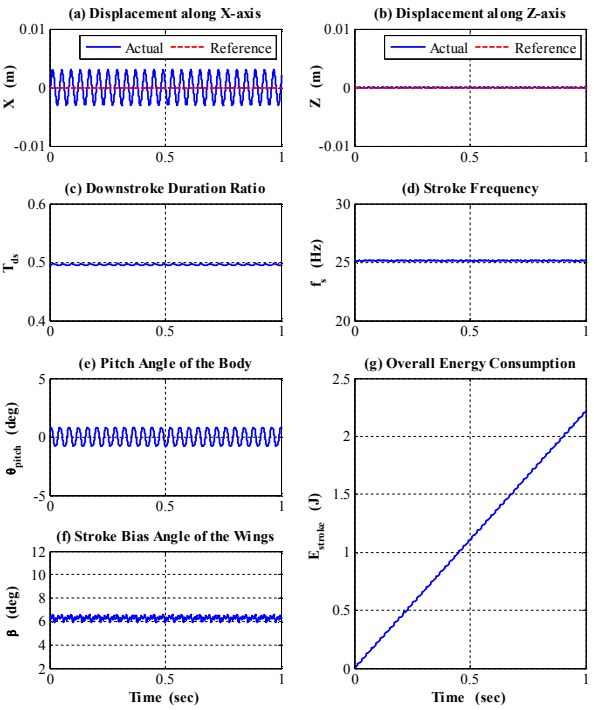

Fig. 11. Simulated results for hovering with controller 2: (a) displacement along X and (b) Z axes, (c) downstroke duration ratio T_{ds}, (d) stroke frequency f_s, (e) pitch angle of the body θ_{pitch}, (f) stroke bias angle of the wings β and (g) overall energy consumption E_{stroke}.

$$E_{TI} = E_{stroke} + 2\int_0^t |P_{TI}|\,dt \tag{33}$$

Based on dimensions of a medium-sized hummingbird, parameters A and R in (12) are set to appropriate values such that $A^2R^6 = 2.5\times10^{-5}$ N^{2}m^2.

A. Hovering

Perhaps, hovering is the most unique flight capability in insects and hummingbirds. Flapping-wing MAVs with a similar stroke pattern are also capable of hovering. Here, hovering of our MAV model over a period of 1 second has been simulated. The results for controllers 1 and 2 are plotted in Fig. 10 and Fig. 11, respectively.

From these diagrams, it is observed that both controllers are able to achieve stable hovering without requiring significant changes in their output values. Since all control outputs remain close to their nominal values, it can be concluded that: 1) pitch profiles in both approaches are close and 2) the value of P_{TI} for controller 1 is insignificant. As a result, both cases should have similar power requirements.

In fact over a hovering period of 1 second, energy consumption with controllers 1 and 2 is estimated to be 2.2116 J and 2.2078 J, respectively (Fig. 10.g and Fig. 11.g). Energy-time profiles in both cases are approximately linear, suggesting a constant energy consumption rate of 2.2116 Watt and 2.2078 Watt, respectively. Note that these values are required to maintain levitation and do not represent cost of transportation.

It is worth mentioning that hummingbirds spend up to 85% of their time sitting and digesting [29]. The rest is spent for various flight activities that often involve foraging. In [30], it has been observed that a 4.3-gram Broad-tailed hummingbird consumes about 7.31 Calories of sugar per day. If the energy consumed at rest is ignored, this amount would be equivalent to an approximate in-flight energy consumption rate of 2.36 Watt which is close to power requirements of our model during hovering.

B. Vertical Takeoff followed by Zigzag Descent

The results of a takeoff/descent maneuver with controllers 1 and 2 are respectively plotted in Fig. 12 and Fig. 13. In these experiments, the hovering model is initially commanded to vertically takeoff such that it reaches an altitude of 10 m within 4 seconds. After one second of hovering at this altitude, the model must descend to a height of 5 m within another 4 seconds. However, reference displacements along X and Z-axes are designed such that this part of the trajectory follows a zigzag pattern (Fig. 12.a-b and Fig. 13.a-b).

This trajectory is designed with two goals in mind. First, considering the importance of vertical takeoff in various MAV applications, it is of interest to investigate the potential for this ability in flapping-wing MAVs. Secondly, following a zigzag pattern demands that both lift and thrust sub-controllers simultaneously apply large changes in their output values (Fig. 12.c-d and Fig. 12.c-d). Such situations are a good opportunity to observe how these sub-controllers

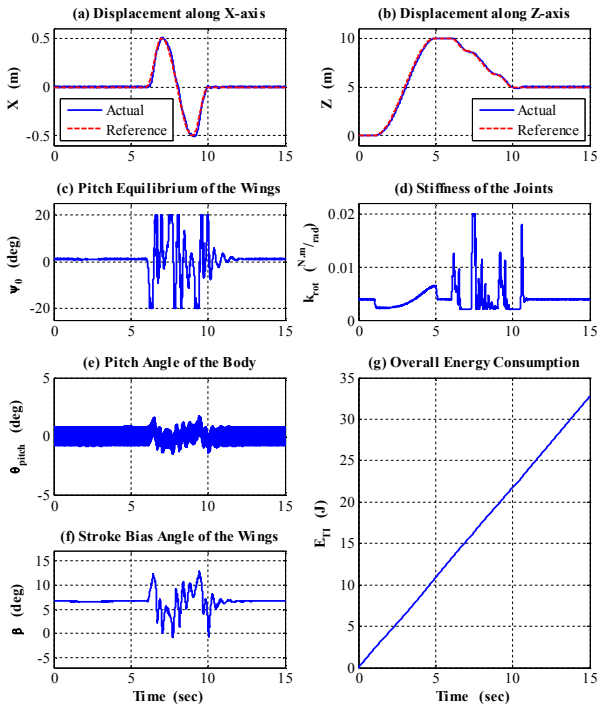

Fig. 12. Simulated results for vertical takeoff and zigzag descent with controller 1: (a) displacement along X and (b) Z axes, (c) pitch equilibrium of the wings ψ_0, (d) stiffness of the joints k_{rot}, (e) pitch angle of the body θ_{pitch}, (f) stroke bias angle of the wings β and (g) overall energy consumption E_{TI}.

affect each other's performance.

The employed control strategies are both able to precisely navigate the model along this trajectory (Fig. 12.a-b and Fig. 13.a-b). Note that during takeoff with controller 1, the outputs of pitch and thrust sub-controllers are almost constant ($t = 1$ sec to $t = 5$ sec in Fig 12.c and f). The same is not true for controller 2 (Fig. 13.c and f). Furthermore, compared to controller 1, it seems the pitch and thrust sub-controllers in controller 2 have to operate at higher frequencies in order to provide the same overall performance. The better response of these sub-controllers in Tunable Impedance approach is in part due to the low degree of coupling between lift and thrust control mechanisms [27].

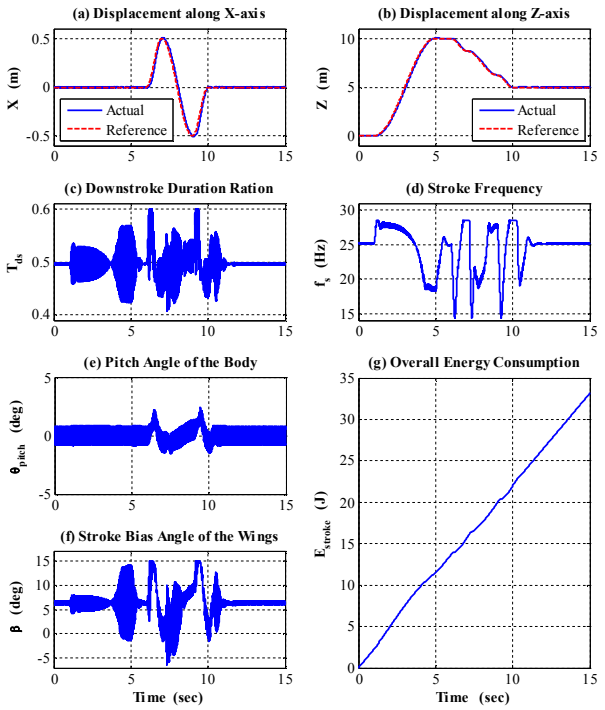

Fig. 13. Simulated results for vertical takeoff and zigzag descent with controller 2: (a) displacement along X and (b) Z axes, (c) downstroke duration ratio T_{ds}, (d) stroke frequency f_s, (e) pitch angle of the body θ_{pitch}, (f) stroke bias angle of the wings β and (g) overall energy consumption E_{stroke}.

Compared to hovering experiments, the model with controller 1 does not demonstrate considerable changes in terms of energy consumption. From Fig. 12.g, average power requirements during takeoff and descent maneuvers are estimated as 2.1651 Watt and 2.1596 Watt, respectively. Note that these values are slightly less than power requirements during hovering. From (12), only a small fraction of overall power (less than 1%) is spent for impedance manipulation (Fig. 12.c-d). The rest, i.e. E_{stroke}, is used to maintain a sinusoidal stroke profile with constant magnitude and frequency. Therefore, from (31)-(32), β and F_D are the only variables that can affect average stroke power requirements. Changes in β are often small and slow (Fig. 12.f). As for F_D it has been previously shown [1] that around k_{op}, smaller values of stiffness decrease the magnitude of this force. Hence, the slight reduction in overall value of E_{stroke} (and E_{TI}) in this experiment is primarily due to changes in stiffness (Fig. 12.d).

Unlike controller 1, controller 2 relies on modification of stroke properties. Thus, (31)-(32) imply that average power requirements in experiments with this controller will depend on desired maneuver. From Fig. 13.g, these requirements during takeoff and descent maneuvers are estimated as 2.3164 Watt and 2.1876 Watt, respectively. The power used for takeoff is approximately 5% more than hovering requirements. Since necessary lift for takeoff is achieved through faster stroke cycles (Fig. 13.d), the increase in energy consumption is to be expected. As for descent, a similar argument can be used to justify the slight reduction in power requirements compared to hovering flight.

C. Forward Flight at Maximum Velocity

Although average flight speed of hummingbirds is about 5-7 m/s, they are known to be able to reach velocities as high as 14 m/s [31]. The thrust boost necessary for such velocities is provided through forward pitching of the body. The downside to this strategy is that it also reduces the maximum possible value of lift; hence, vertical maneuvers at such velocities are very challenging.

The presented flapping-wing MAV model also demonstrates such behavior with both controller 1 and 2. Here, the model can reach velocities as high as 10 m/s

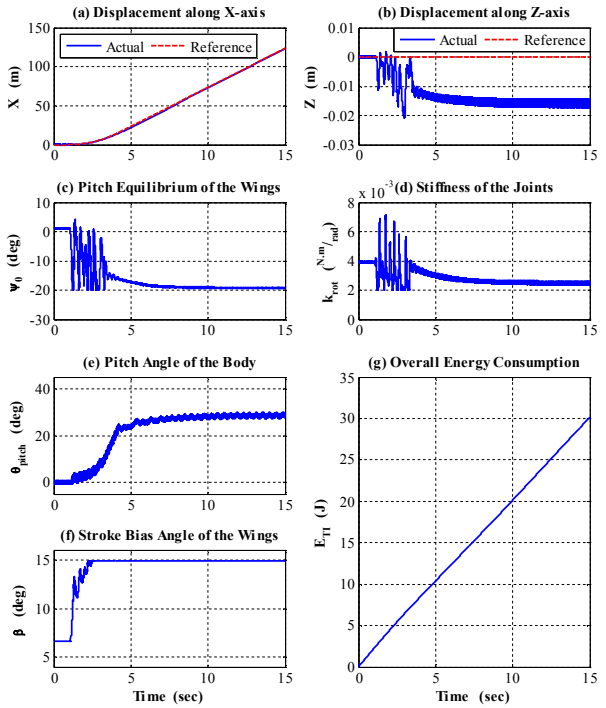

Fig. 14. Simulated results for forward flight at 10 m/s with controller 1: (a) displacement along X and (b) Z axes, (c) pitch equilibrium of the wings ψ_0, (d) stiffness of the joints k_{rot}, (e) pitch angle of the body θ_{pitch}, (f) stroke bias angle of the wings β and (g) overall energy consumption E_{TI}.

before lift sub-controllers fail to stabilize its altitude. The simulated results with controller 1 and 2 at 10 m/s are illustrated in Fig. 14 and Fig. 15, respectively. In both cases, the strained performance of lift sub-controller results

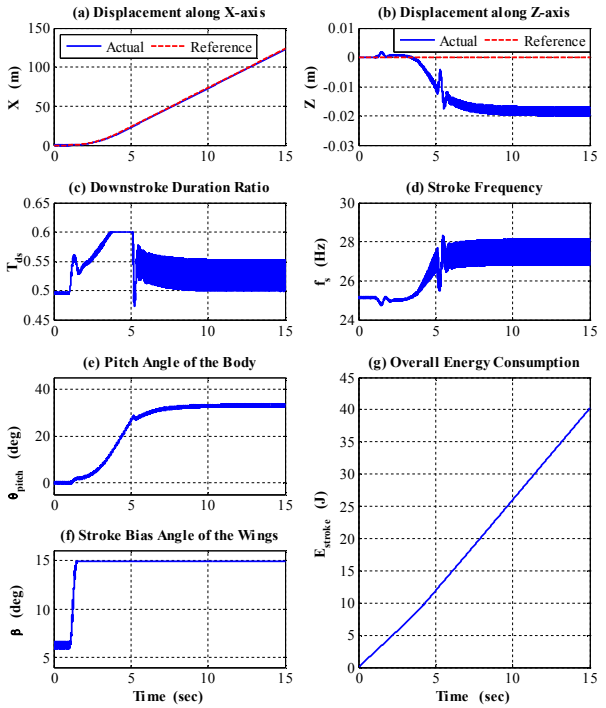

Fig. 15. Simulated results for forward flight at 10 m/s with controller 2: (a) displacement along X and (b) Z axes, (c) downstroke duration ratio T_{ds}, (d) stroke frequency f_s, (e) pitch angle of the body θ_{pitch}, (f) stroke bias angle of the wings β and (g) overall energy consumption E_{stroke}.

in a slight altitude loss (Fig. 14.b and Fig. 15.b).

From Fig. 14.g, the model with controller 1 requires only 2.0018 Watt to maintain its target velocity. This value is 9.5% lower than the power required for hovering. Similar to the takeoff experiment in Section V.B, this reduction is caused by lowered values of stiffness (Fig. 14.d).

The model with controller 2 reaches target velocity through employing higher values of stroke frequency (Fig. 15.d). From Fig. 15.g, this approach requires 2.8541 Watt which is 29.3% larger than the power required for hovering. Note that for the same maneuver with controller 1, required power is reduced by 0.8523 Watt, i.e. almost 30%.

VI. Conclusion

Inspired by insect flight muscles, Tunable Impedance is a semi-passive method for regulation of aerodynamic forces in flapping-wing MAVs [1]. From (25), pitch rotation profile of each wing depends on mechanical impedance properties of its joint. The shape of this profile determines how wing's angle of attack changes and consequently, how much lift and thrust is produced. Therefore, manipulation of mechanical impedance properties can indirectly influence average values of these aerodynamic forces (Fig. 5).

Compared to conventional methods of force control, the primary advantage of this approach is that it requires no modification in stroke profiles of either wing. In fact, both wings can use the same sinusoidal pattern of flapping with fixed parameters – except for stroke bias angle β which is an independent control parameter. Furthermore, it has been previously shown that by low-frequency manipulation of mechanical impedance properties, i.e. within a bandwidth limited by stroke frequency f_s, coupling between changes in lift and thrust is considerably reduced [27].

These advantages effectively simplify the control system and can reduce the amount of onboard hardware required in an actual MAV. The results presented in [26]-[27] demonstrate that through Tunable Impedance approach, a high degree of controllability is achievable and hence, the MAV will be able to handle various agile and complex maneuvers.

In this work, we investigated the impact of Tunable Impedance approach on power requirements of a flapping-wing MAV. It has been observed that the necessary amount of energy for impedance manipulation is a lot smaller than the amount required for stroke motion. Since stroke profile is approximately constant, the total power requirement is almost independent of desired maneuver. For the simulated MAV model in this paper, the required power is always less than 2.21 Watt. Interestingly, this value is in agreement with average in-flight energy consumption rate of a hummingbird with similar body dimensions.

In comparison, control approaches that rely on modification of stroke properties often require considerably

greater amounts of power. This increase in power consumption is specially observed when a maneuver demands more lift or thrust production (e.g. acceleration in Fig. 15.a) which is fulfilled via employing faster stroke motions.

The gap in energy consumption will widen further when we consider the case in which pitch rotation of the wing is not governed by a passive mechanism [32]. Consequently, additional actuators are required to directly rotate the wing and modify its angle of attack throughout each stroke cycle. From (14) and (24), one can estimate the active torque $\tau_\psi = \tau_{ext}$ that must be applied to each wing so that it follows a predefined pitch profile ψ. The energy required for active pitch rotation of both wings, i.e. E_ψ is then calculated as:

$$E_\psi = 2\int_0^t |\, \tau_\psi \, \dot{\psi} \,|\, dt \tag{34}$$

From (34), if the model with controller 2 were to actively generate the same wing pitch profiles as the simulations in Section V, its power requirements would increase by 0.5571 Watt during hovering, 0.6613 Watt during takeoff and 0.9540 Watt when moving forward at 10 m/s.

As a bio-inspired control strategy with low power demands, the Tunable Impedance method is a promising solution to both problems of maneuverability and power efficiency in flapping-wing MAVs. Considering the limitations of available batteries, implementation of this approach may greatly improve flight time. Our current work is focused on development of appropriate actuators for impedance manipulation. Above all, such actuators must have minimized loading effects so that wing's dynamics are not significantly perturbed. Upon achieving satisfactory results in impedance manipulation, our eventual goal is to install the designed actuators on a 3-inch-wingspan flapping-wing MAV and conduct actual flight experiments.

REFERENCES

[1] H. Mahjoubi, and K. Byl, "Modeling synchronous muscle function in insect flight: a bio-inspired approach to force control in flapping-wing MAVs," *J. Int. & Robotic Systems*, 70 (1-4), pp. 181-202, 2013. (Available Online, DOI: http://dx.doi.org/10.1007/s10846-012-9746-x)

[2] K.L.B. Cook, "The silent force multiplier: the history and role of UAVs in warfare," in Proc. IEEE Aerospace Conf., pp. 1-7, March 3-10, 2007.

[3] R. J. Wood, "The first takeoff of a biologically inspired at-scale robotic insect," *IEEE Transactions on Robotics*, 24, pp. 341–347, 2008.

[4] G.C.H.E. de Croon, K.M.E. de Clerq, R. Ruijsink, B. Remes, and C. de Wagter, "Design, aerodynamics, and vision-based control of the DelFly" *International Journal of Micro Air Vehicles*, 1 (2), pp. 71-97, 2009.

[5] R. Michelson, D. Helmick, S. Reece, C. Amarena, "A reciprocating chemical muscle (RCM) for micro air vehicle 'Entomopter' flight," In Proceedings of the Association for Unmanned Vehicle Systems International (AUVSI), pp. 429-443, 1997.

[6] R. Michelson, "The Entomopter," in *Neurotechnology for Biomimetic Robots*. The MIT Press, 2002, pp. 481-509.

[7] H. Mahjoubi, and K. Byl, "Tunable impedance: a semi-passive approach to practical motion control of insect-inspired MAVs," in Proc. IEEE Int. Conf. Robotics and Automation (ICRA), pp. 4621-4628, May 14-18, 2012.

[8] R. Dudley, *The Biomechanics of Insect Flight: Form, Function, Evolution*. Princeton University Press, 2000.

[9] H. Mahjoubi, and K. Byl, "Insect flight muscles: inspirations for motion control in flapping-wing MAVs," in Proc. Int. Conf. Unmanned Aircraft Systems (ICUAS), June 12-15, 2012.

[10] H. Mahjoubi, and K. Byl, "Analysis of a tunable impedance method for practical control of insect-inspired flapping-wing MAVs," In Proc. IEEE Conf. on Decision and Control and European Control Conf. (CDC-ECC), pp. 3539-3546, December 12-15, 2011.

[11] T. Miura, T. Shirai, and T. Tomioka, "Proposal of joint stiffness adjustment mechanism SAT," JSME Conference on Robotics and Mechatronics '02, pp. 29, 2002. (in Japanese)

[12] G. Tonietti, R. Schiavi, and A. Bicchi, "Design and control of a variable stiffness actuator for safe and fast physical human/robot interaction," 2005 IEEE International Conference on Robotics and Automation (ICRA), Barcelona, Spain, April 2005.

[13] R. Schiavi, G. Grioli, S. Sen, and A. Bicchi, "VSA-II: a novel prototype of variable stiffness actuator for safe and performing robots interacting with humans," 2008 IEEE International Conference on Robotics and Automation (ICRA), Pasadena, CA, USA, May 19-23, 2008.

[14] J. Choi, S. Hong, W. Lee, S. Kang, and M. Kim, "A robot joint with variable stiffness using leaf springs," *IEEE Transactions on Robotics*, 27 (2), pp. 229-238, April 2011.

[15] "Insect Wings," Internet: www.amentsoc.org/insects/fact-files/wings.html, 1997 [February 22, 2013].

[16] A. B. Schultz, J. A. Faulkner, and V. A. Kadhiresan, "A simple hill element-nonlinear spring model of muscle contraction biomechanics," *Journal of Applied Physiology*, 70 (2), pp. 803-812, 1991.

[17] M. H. Dickinson, "The effects of wing rotation on unsteady aerodynamic performance at low Reynolds numbers," *Journal of Experimental Biology*, 192, pp. 179-206, 1994.

[18] M. H. Dickinson, F. Lehmann, and S. P. Sane, "Wing rotation and the aerodynamic basis of insect flight," *Science*, 284 (5422), pp. 1954-1960, 1999.

[19] C. P. Ellington, "The aerodynamic of hovering insect flight I. the quasi-steady analysis," *Philosophical Transactions of the Royal Society of London*, 305 (1122), pp. 1-15, 1984.

[20] A. Willmott, C. Ellington, C. van den Berg, and A. Thomas, "Flow visualisation and unsteady aerodynamics in the flight of the hawkmoth *Manduca sexta*," *Philosophical Transactions of the Royal Society of London*, *B Biological Sciences*, 352, pp. 303-316, 1997.

[21] S. Sane, "The aerodynamics of insect flight," *Journal of Experimental Biology*, 206, pp. 4191-4208, 2003.

[22] X. Deng, L. Schenato, W. C. Wu, and S. S. Sastry, "Flapping flight for biomimetic robotic insects: part I–system modeling," *IEEE Transactions on Robotics*, 22 (4), pp. 776–788, 2006.

[23] Y. Fung, *An Introduction to the Theory of Aeroelasticity*, New York: Dover, 1969.

[24] S. P. Sane, and M. H. Dickinson, "The control of flight by a flapping wing: lift and drag production," *Journal of Experimental Biology*, 204, pp. 2607-2626, 2001.

[25] W. B. Dickson, and M. H. Dickinson, "The effect of advance ratio on the aerodynamics of revolving wings," *Journal of Experimental Biology*, 207, pp. 4269-4281, 2004.

[26] H. Mahjoubi, and K. Byl, "Steering and horizontal motion control in insect-inspired flapping-wing MAVs: the tunable impedance approach," in Proc. American Control Conference (ACC), pp. 901-908, June 27-29, 2012.

[27] H. Mahjoubi, and K. Byl, "Trajectory tracking in sagittal plane: decoupled lift/thrust control via tunable impedance approach in flapping-wing MAVs," To appear in Proc. American Control Conference (ACC), June 17-19, 2013.

[28] D. B. Doman, and M. W. Oppenheimer, "Dynamics and control of a minimally actuated biomimetic vehicle: part I. aerodynamic model," AIAA Guidance, Navigation, and Control Conference, San Francisco, California, USA, 10-13 August, 2009.

[29] L. L. Wolf, and F. R. Hainsworth, "Time and energy budgets of territorial hummingbirds," *Ecology*, 52 (6), pp. 980-988, 1971.

[30] O. P. Pearson, "The daily energy requirements of a wild Anna hummingbird," *The Condor*, 56 (6), pp. 317-322, 1954.

[31] F. B. Gill, "Hummingbird flight speeds," *The Auk*, 102 (1), pp. 97-101, 1985.

[32] B. Yin, and H. Luo, "Effect of wing inertia on hovering performance of flexible flapping wings," *Physics of Fluids*, 22 (11): 111902, 2010.